# CHAPTER - 2

# THEORITICAL BACKGROUND AND EXPERIMENTAL TECHNIQUES

## 2.1 Introduction

The primary characteristics of a ferrite material for MLCI applications as discussed in chapter 1 are reasonable saturation magnetization, high permeability in the radio frequency range, high resistivity, high Curie temperature, fine grains, low dielectric constant, low losses and high quality factor. The ferrite material could be made suitable for high frequency MLCI applications by modifying the structural, magnetic and electrical properties. The properties are highly sensitive to the method of preparation, the kind and the amount of impurity added and the annealing heat treatment. Enhancement in magnetic and electrical properties can be achieved by processing the Ni-Zn ferrite in nanoform under stringent appropriate conditions [**1, 2**]. In order to understand the nature of the mechanisms involved in controlling various properties associated with MLCI applications, it is necessary to have a thorough knowledge of the ferrite structure, which has been presented in the following section.

## 2.2 Ferrite Structure

Ferrites are ceramic magnetic materials which have the general formula $AB_2O_4$ [**3, 4**], where A and B represent metal ions. Ferrites crystallize into spinel structure, which is named after the mineral spinel, [**5**] $MgAl_2O_4$. The spinel crystal structure is determined primarily by the oxygen ions lattice. The elementary cell of a spinel lattice contains eight molecules of $AB_2O_4$ in which 32 oxygen ions form cubic close packed structure leaving 96 available interstitial sites. Out of these 96 interstitial sites, 64 are tetrahedral (A) and 32 are octahedral (B) and each site is surrounded by four and six oxygen ions respectively. These sites are only partially occupied by 24 metal ions. The arrangement of the ions in a complete ordered ferrite is shown in Fig.2.1.

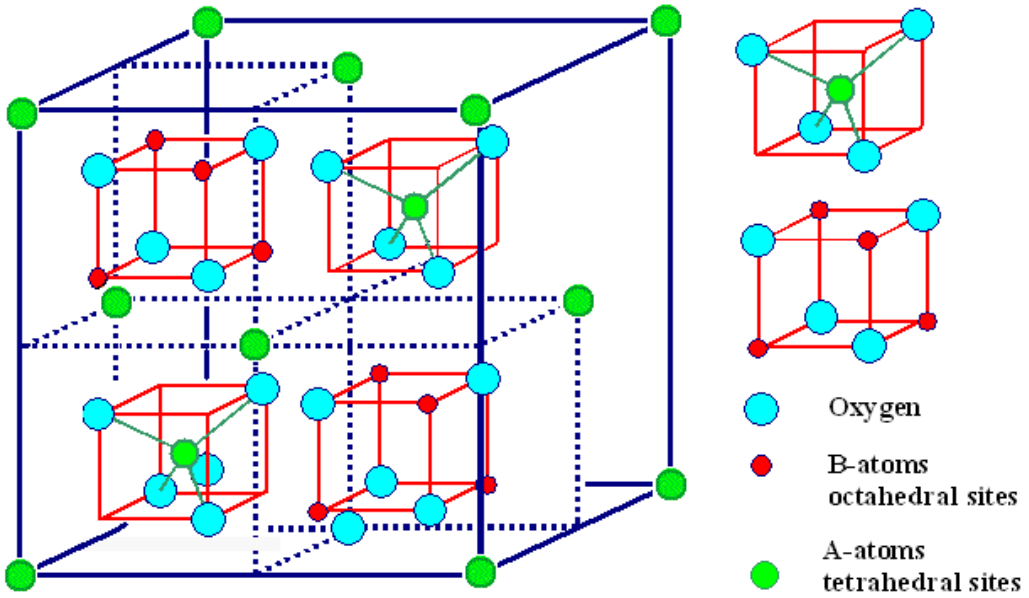


**$AB_2O_4$ spinel** The red cubes are also contained in the back half of the unit cell

*Figure 2.1: Spinel structure with the representative tetrahedral (A) and octahedral [B] sites in the unit cell.*

Among ferrites there are three classes; namely, normal, inverse and mixed ferrites. In normal ferrites the tetrahedral sites are occupied by only the divalent ions and the octahedral sites are occupied by the trivalent ions only. The distribution is represented by the general formula $(A^{2+})\ [B_2{}^{3+}]\ O_4$. The first pair of brackets encloses ions on A-sites and the second pair on B-sites. These ferrites are not magnetic. Examples of such ferrites are zinc ferrite $ZnFe_2O_4$ and cadmium ferrite $CdFe_2O_4$. In inverse ferrites 8 out of 16 trivalent ions occupy tetrahedral sites and the octahedral sites are occupied both by divalent ions and the remaining trivalent ions. The distribution is represented by the general formula $(B^{3+})\ [A^{2+}\ B^{3+}]\ O_4$. Magnetite and nickel ferrite fall in this category.

For mixed ferrites, both A and B sites are occupied both by divalent and trivalent ions. The ion distribution in this case is represented by the general formula $(A_a{}^{2+}\ B_{1-a}{}^{3+})\ [A_{1-a}{}^{2+}B_{1+a}{}^{3+}]O_4{}^{-2}$ examples are zinc-manganese ferrite and nickel-zinc ferrite.

The factors which can influence the distribution of the metal ions over the A and B sites are i) their ionic radii and electronic configuration of the metal ions and ii) the electrostatic energy of the spinel lattice.

**2.3 Measuring techniques**

The performance of a ferrite system useful for a particular application is always decided by its properties. The material should be subjected to different tests to procure information about the properties. The development of the system with all good properties is based upon the analysis of vast amount of experimental data available from various techniques. The appropriate techniques which yield quality information on various properties needed for the understanding of MLCI applications have been discussed in the following sections.

**a) X-ray diffractometer**

X-ray diffraction, a well known technique used for the identification of the material phases, crystal structure, d-spacing, determination of average crystallite size and lattice constant [**6**]. Powder X-ray diffraction measurements for all the samples have been taken on Rigaku X-ray diffractometer using Cu Kα radiation (1.5406 Å) and Inel Equinox-3000 using Co-$K_\alpha$ radiation (1.7889 Å) at lowest scan rate of $0.02^o$ per minute.

**b) Scanning electron microscopy**

The SEM is one of the most versatile instruments available for the examination and analysis of the microstructural characteristics of the fractured surfaces of solid objects. The grain size could be determined with this technique. The coupling of an energy-dispersive x-ray detector to an SEM makes it possible to obtain higher magnification, larger depth of field, greater resolution, topographic, crystallographic, and compositional information rapidly, efficiently, and simultaneously for the same area**.**

Scanning electron microscope (JEOL – JSM 6360) equipped with “Tungsten” filament was used to record photomicrographs of pellets whose surfaces were coated with a thin layer of platinum. In order to be observed with a SEM, objects are first made conductive for current. This is done by coating them with an extremely thin layer (1.5 - 3.0 nm) of gold or gold-palladium or

platinum. The grain size calculations were made possible in high temperature treated samples using Cottrell's formula [**7**].

**c) Field emission scanning electron microscopy**

**Field emission microscopy** (FEM) is an analytical technique for high resolution imaging with high brightness sources, small probes and short working distances used in materials science to investigate molecular surface structures and their electronic properties and were invented by Erwin Wilhelm Muller. Field emission was explained as quantum tunneling of electrons in the late 1928s by Fowler and Nordheim for bulk metals and with slight modification for other bulk crystalline solids.

The FEM was one of the first surface analysis instruments that approached near atomic resolution used to produce real space magnified images of a surface showing what it looks like (surface crystallography i.e. how the atoms are arranged at the surface, surface morphology i.e. the shape and size of topographic features making the surface and surface composition). The microstructure was studied using SUPRA 55 Zeiss with a primary $e^-$ beam at an enegy of 25 K eV.

**d) Transmission electron eicroscope**

The transmission electron microscopic technique (TEM) is used to obtain structural information from the samples that are very much thin to transmit electrons. For the observation of the nanoparticles; samples were fixed in 2.5% - 3% gluteraldehyde in 0.1M phosphate buffer (pH = 7.2) for 24h at 4oC an post fixed in 2% aqueous osmium tetroxide in the same buffer for 2 h. Dehydrated in series of graded alcohols, infiltrate and embedded in araldite 6005 resin. Ultra thin (50-70nm) sections were made with a glass knife on ultra microtome, mounted on cooper grids and stained with saturated aqueous uranyl acetate and counter stained with Reynolds lead citrate and the same has been viewed under PHILIPS CM200(Operating voltages : 20-200kv Resolution :2.4 $A^o$) at required magnifications.

**e) Mossbauer spectrometer**

The analysis of Mossbauer spectra provides an accurate estimation about the valence state of iron ions, their environment and the magnetic interactions taking place among these ions

in a material. Mossbauer spectra for all samples were recorded in constant acceleration mode. The source used was 25 mCi $Co^{57}$ in rhodium matrix. The spectrometer was calibrated using a standard natural iron foil as a reference material. The spectra have been recorded at room temperature and low temperatures (300 K and 5 K) without applying any external magnetic field and in the presence of 5 T external field parallel to the direction of γ- rays at 5K.

**f) FT IR spectrometer**

FT IR spectra of finely crushed powder of all the compositions were recorded for the all samples in the range - 3000 $cm^{-1}$ to 400 $cm^{-1}$ on MAGNA 550 Nicolet Instruments Corporation wherein KBr is used as solvent in 1 : 3 proportion. The spectrum, transmittance (%) against wave number ($cm^{-1}$) has been used for the interpretation of the result.

**g) Vibration sample magnetometer**

Room temperature magnetization of the sample was measured using a Vibrational sample Magnetometer (115 PAR-EG&G Model) under an external magnetic field of 20 kOe. Low temperature measurements were performed using Quantum design Physical Properties Measuring System at 10K temperature under an external magnetic field of strength 20kOe.

The Curie temperature of the samples in powder form has been determined from the magnetization versus temperature graphs. The accuracy of the measurement was found to be about ± 2 $^{o}$C.

Another simple experimental set-up described by Sohoo [**8**] was used to determine the Curie temperature of the sample. A small piece of the ferrite sample (~ 50 mg ) was attached to the lower end of an iron rod and the upper end of which was placed in contact with a powerful electromagnet. The lower end of the rod carrying the sample was kept inside a Quartz tube furnace (on which a super kanthol wire was wound to heat the tube) the temperature of which was gradually raised till the material transformed from ferromagnetic to paramagnetic. The temperature at which the ferrite sample falls due to loss of it's magnetization represents the Curie temperature. This temperature was measured using chromel-alumel thermocouple. The accuracy of the measurement was found to be about ± 2 $^{o}$C.

**h) Impedance analyzer**

The inductance (L) was measured using HP4192A LF Impedance analyzer and at the small voltage of 1mV from 1 kHz to 1 MHz. Using the value of L initial permeability at different frequencies was computed as $\mu_i = \frac{L}{L_o}$ where $L_o$ is the air core inductance $= 0.4606 N^2 h \log\left(\frac{OD}{ID}\right) microhenry$[**9**] and N is the number of turns. 20 turns of 30SWG enameled copper wire were wound on the sintered toroidal samples of average dimensions: outer diameter (OD) = 12mm, inner diameter (ID) = 8mm; thickness (h) = 4.5mm for measuring the inductance.

**i) Two probe method**

DC resistivity measurements of the samples were made by the two-terminal-dc method. Although four-probe method is considered better as compared to two-probe method as far as contact resistance is concerned, yet two-probe method was preferred since it gives more accurate value of the bulk resistivity of the material.

Freshly ground, dry and clean pellets coated with silver paste to have good ohmic contact were placed in between the two electrodes of the measurement cell. A known dc voltage V was applied across the two surfaces of the sample whose dimensions are 16 mm in diameter and 4 mm in thickness. The electric field (E = 1 V/m) applied was kept constant for all the samples. The value of current, I, passing through the sample was measured using Digital Nano-ammeter model DNM-121. The resistance *R* and the resistivity $\rho$ of the samples were calculated using the relations

$$R = \frac{V}{I}$$

$$\rho = R\left(\frac{A}{t}\right)$$

Here *A* is the area of cross section and *t* is the thickness of the pellet. For temperature variation of resistivity the cell containing the sample was kept in a furnace and maintained at the desired

temperature with the help of a temperature controller. Sufficient time was given at each temperature so that the sample may attain the equilibrium temperature. At this stage, the above procedure was repeated to evaluate the resistivity of the sample from room temperature to 200$^{o}$C.

**j) Archimedes principle**

The experimental density d, of the all the samples was determined using the Archimedes's principle. Density of a sample varies with sintering temperature and sintering time.

$$d = \frac{w_a}{w_a - w_w}$$

Here $w_a$ is the weight of the sample in air, $w_w$ is the weight of the sample in water.

Theoretical density or X-ray density $d_x$ was calculated from the values of lattice constant using the following relation

$$d_x = \frac{8M}{Na^3}$$

Here $M$ is the molecular weight of the ferrite sample, $N$ is the Avogadro number, $a$ is the lattice constant. From the values of X-ray and experimental densities the % of porosity of the samples were calculated using the relation

$$Porosity = \left(1 - \frac{d}{d_x}\right) 100\,\%$$

**2.4 Theoretical background**

The analysis of vast experimental data obtained from several techniques related to properties of the material requires the theoretical aspects of various phenomena. The variations in several properties require theoretical background of the concepts for their plausible interpretation. The necessary theoretical background of the various techniques and related concepts needed for understanding the changes in the structural, magnetic and electrical properties have been presented in the following section.

**A. Structural Properties**

**a) X –ray diffraction**

X-ray diffraction patterns of powder compositions give information about the information of single phase spinel structure, d-spacing of crystal planes, crystallite size and lattice constant from the observed diffraction angles [**6**]. The peak intensity in X-ray diffraction patterns is proportional to scattering power of atoms occupying a crystal plane and depends on the distribution of cations among the tetrahedral (A) and octahedral (B) sites. [**10**]. Comparing the peak intensities from the experimentally obtained X ray diffraction patterns with the calculated intensities for the proposed cation distributions using the equation [**6**], one can obtain exact cation distribution.

$$I_{hkl} = |F|^2_{hkl} . p . L_p$$

where $F$ is structure factor, $p$ is multiplicity factor and $L_p$ is Lorentz-polarization factor.
The structure factor for each plane can be calculated using the equation.

$$|F|^2_{hkl} = \left( \sum_{i=1}^{56} f_i \sin 2\pi(hu_i + kv_i + lw_i) \right)^2 + \left( \sum_{i=1}^{56} f_i \cos 2\pi(hu_i + kv_i + lw_i) \right)^2$$

where $f_i$ is atomic scattering factor, $h$, $k$ and $l$ are Miller indices of a plane and $u$, $v$ and $w$ are atomic coordinates in a plane. The number 56 represents the total number of cations and anions required for forming the unit cell of spinel.

The calculation of structure factor requires knowledge about the ideal locations of ions in the unit cell. The peak intensities can be calculated by substituting the geometrical coordinates and scattering factors of atoms into the above equations.

**b) Field emission scanning electron microscopy**

An FESEM is used to visualize very small topographic details on the surface or entire fractioned objects that may be as small as 1nm. Electrons are liberated from a field emission source and accelerated in a high electrical field gradient. Within the high vacuum column these so-called primary electrons are focussed and deflected by electronic lenses to produce a narrow scan beam that bombards the object. As a result secondary electrons are emitted from each spot on the object. The angle and velocity of these secondary electrons relates to the surface structure

of the object. A detector catches the secondary electrons and produces an electronic signal. This signal is amplified and transformed to a video scan-image that can be seen on a monitor or to a digital image that can be saved and processed further.

In standard electrom microscopes the electrons are mostly generated by heating a tungsten filament but in a field emission (FE) scanning electron microscope no heating but a so-called "cold" source is employed. An extremely thin and sharp tungsten needle (tip diameter 10–7–10-8 m) functions as a cathode in front of a primary and secondary anode. The voltage between cathode and anode is in the order of magnitude of 0.5 to 30 KV. Because the electron beam produced by the FE source is about 1000 times smaller than in a standard microscope, the image quality is markedly better, clearer, less distorted along with high spatial resolution. For ultra high magnification imaging In- lens FESEM is used. Further smaller area contamination spots can be observed with energy dispersive X-ray spectroscopy. EDS identifies the elemental composition of materials imaged in SEM. In contrast to a conventional tungsten filament, a FE tip lasts theoretically for a life time provided the vacuum is maintained stable.

**c) Mössbauer spectroscopy**

Mössbauer spectroscopic technique is widely used to determine the chemical, structural, magnetic and time-dependent properties of a material and primarily the valence state of iron ions. Mössbauer effect is an example of resonance fluorescence. Resonance fluorescence occurs when a photon, resulting from the de excitation of a system from state B to state A, excites an identical system from state A to state B. This phenomenon is common for optical photons and sound waves, but resonance absorption of nuclear γ- rays, prior to Mössbauer work, was difficult to detect experimentally. This was because the sum of the recoil energy given to the emitting and to the absorbing nuclei (subtracted from the emitted γ- ray energy) in order to conserve momentum during emission and absorption is large enough so that the emitted energy spectrum usually does not strongly overlap the absorption line. Also, thermal motions broadened the spectra and reduced the absorption cross section at resonance. In 1957 Mossbauer [**11**] observed the resonance fluorescence in $Ir^{191}$ in which case the recoil energy is 0.05e.v.and the thermal broadening is 0.1e.v. Mössbauer cooled both the source and the absorber in order to reduce the Doppler broadening. He, however, observed that the resonance fluorescence increased with

decreasing temperature. He explained his results by recognizing that when the source is cooled; an increased fraction of γ- rays is emitted for which the recoil momentum is given to the entire crystal instead of to a single nucleus. The crystal is much more massive than a nucleus and gains a negligible amount of recoil energy in absorbing the recoil momentum; therefore the γ- ray has essentially the total energy of the transition. Thus the process is called recoilless [**9**]. Similarly, a recoilless absorption process takes place when the nuclei are bound in a crystal lattice at a sufficiently low temperature (temperature below the Debey characteristic temperature). A very important characteristic of these recoilless processes is that they are not Doppler broadened by thermal vibrations, and therefore they exhibit the natural line width of the transition. An alternate measure of the line width is obtained by considering the ratio of the width of the line to its energy. For Mössbauer isotope $Fe^{57}$, this fractional width is $10^{-13}$. This means that the energy of γ- ray is defined to one part in $10^{+13}$ which makes it the most accurately defined electromagnetic radiation available for physical measurements.

In solids there are various hyperfine interactions that perturb the nuclear energy levels and the principle use of the Mössbauer effect is to study these interactions. Magnetic and quadrupole interactions lift the $I_Z$ degeneracy of the nuclear ground and excited states and cause the energy levels to split. In addition there is an electric monopole interaction, called the Mössbauer effect isomer shift, which shifts the centre of gravity of the Mössbauer spectrum which is a plot of γ-ray transmission versus Doppler velocity between the source and the absorber.

The following parameters are extracted from a Mossbauer spectrum to draw meaningful conclusions about the nature of the sample under study.

i. Isomer shift
ii. Quadruple splitting
iii. Magnetic hyperfine splitting
iv. Line shape and line width

**i. Isomer shift**

The isomer shift is essentially the result of electric monopole interaction and arises because of the fact that the ground and excited states of the nucleus have different effective charge radii. If the source and the absorber are in the same matrix and at the same temperature,

the transition energies will be identical and absorption will occur when the relative velocity between the source and the absorber is zero. If, however, the two matrices are not identical, which is the case in general; one would expect a slight difference in the transition energies in the source and that in the absorber. This energy difference is called the isomer shift or chemical shift. Since only a difference in source and absorber energies is measured, both the source and absorber materials must be specified for the isomer shift to be meaningful. It has been shown that the change in the nuclear energy levels is the result of change in S- electron density at the nucleus. The isomer shift can be written in the form [**13**];

Isomer shift = $\frac{2\pi}{5} Z e^2 \left[\psi^2{}_a(0) - \psi^2{}_b(0)\right]\left[R^2{}_{ex} - R^2{}_{gd}\right]$

Where $R_{ex}$ and $R_{gd}$ are nuclear radii of ground and excited states and -e $\psi^2(0)$ is the electronic charge density at the nucleus.

As the isomer shift is very sensitive to the s-electron density, the results of the isomer shift measurements would give information about the degree of covalence and ionic valence state of Mössbauer isotopes.

**ii. Quadrupole interaction**

The electrostatic interaction of nuclear quadrupole moment with the surrounding electronic charge is the electric quadrupole interaction [**14**]. The nuclear quadrupole moment (Q) interacts with the electric field gradient (EFG) and gives rise to a hyperfine structure. The gradient of the electric field on the nucleus is generated both by atomic electrons and by the ions which surround the atoms. The nuclear quadrupole coupling is expressed by the Hamiltonian

$$H = \frac{e^2 Q q}{4I(2I-1)}\left[3I_z^2 - \frac{\eta}{2}\left(I_+^2 - I_-^2\right)\right]$$

Where q is the electric field gradient at the nucleus, $I_+$ and $I_-$ are the raising and lowering operators and η is the asymmetry parameter defined by

$$\eta = \frac{V_{xx} - V_{yy}}{V_{zz}}$$

The components of EFG are usually chosen so that $|V_{zz}| \geq |V_{xx}| \geq |V_{yy}|$ making $0 \leq \eta \leq 1$ .

The solution of the secular equation corresponding to the above equation gives

$$E_Q(m_I) = \frac{e^2 Qq}{4I(2I-1)}\left[3m_I^2 - I(I+1)\right]\left(1+\frac{1}{3}\eta^2\right)^{\frac{1}{2}}$$
$$m_I = I, I-1, -----$$

Nuclei with spins I = 0 and I = ½ have spherically symmetric charge distribution, and the quadrupole moment Q is zero. Therefore the nuclear levels having spin I = 0, ½ will not be split by the quadrupole interaction. For $Fe^{57}$ nucleus the excited state (I =3/2) is split in to two lattice states, while the ground state (I =1/2) remains unsplit.

When the crystal has axial symmetry (η =0), the sublevels are characterized by a definite $m_I$ value and the states of $\pm m_I$ are degenerate. The energy shifts are given by [**15**]

$$E_Q(m_I) = \frac{e^2 Qq}{4I(2I-1)}\left[3m_I^2 - I(I+1)\right]$$

For this case the angular dependence of the transition probabilities are $\frac{3}{2}\left(1+Cos^2\theta\right)$ and $\left(1+\frac{3}{2}Cos^2\theta\right)$ for $\pm\frac{3}{2} \rightarrow \pm\frac{1}{2}$ and $\pm\frac{1}{2} \rightarrow \pm\frac{1}{2}$ transitions respectively, where θ is the angle between the gamma ray and the axis of symmetry. For polycrystalline absorbers the angle between the symmetry axis and the direction of observation is random and the intensities of two lines are equal. However, if a single crystal is used the intensities of the two lines are different and depend on the angle θ. The inequality of the relative intensities (θ = 0, 3:1; θ = 90, 3:5) provides the simplest method of determining the sign of quadrupole coupling $e^2qQ$. When the crystal does not have axial symmetry ($\eta \neq 0$), $m_I$ is no longer a good quantum number. The solution of the secular equation for the Hamiltonian gives, for I = 3/2, $E_Q(m_I) = \frac{e^2 Qq}{4I}\left(1+\frac{1}{3}\eta^2\right)^{\frac{1}{2}}$, making it difficult to determine the magnitude of $e^2qQ$ unless η is known. Large values of η tend to make the intensities of two lines equal [**16**]

The Q interaction measurements give an indication of the co-ordination number at the Mössbauer site in the sample studied and reveal information regarding the crystal fields.

**iii. Magnetic hyperfine interaction**

The interaction between the nuclear magnetic moment μ and a magnetic field H, which may be an externally applied field or a local effective field, is described by the Hamiltonian

$H_m = -\vec{\mu}.\vec{H} = -g\,\mu_n H I_Z$ where g is the gyro magnetic ratio and $\mu_n$ the nuclear magnetic moment. The eigen values of the Hamiltonian are given by

$E_m = -\,g\,\mu_n\,H\,m_I$ , where $m_I$ can have values –I, -I+1, ----------,I-1,I.

The magnetic field, therefore, splits a nucleus of spin I into (2I+1) sublevels. The sublevels are separated by $\Delta E_m = g\,\mu_n\,H$ . The hyperfine splittings of I=3/2 and I=1/2 levels of $Fe^{57}$ are shown in Fig 5. In Iron compounds below magnetic ordering temperature, the $Fe^{57}$ nucleus experiences an effective internal field. Although it is possible to create large enough fields by external means to cause splitting, the latter is caused by the electrons on the Mössbauer atom itself.

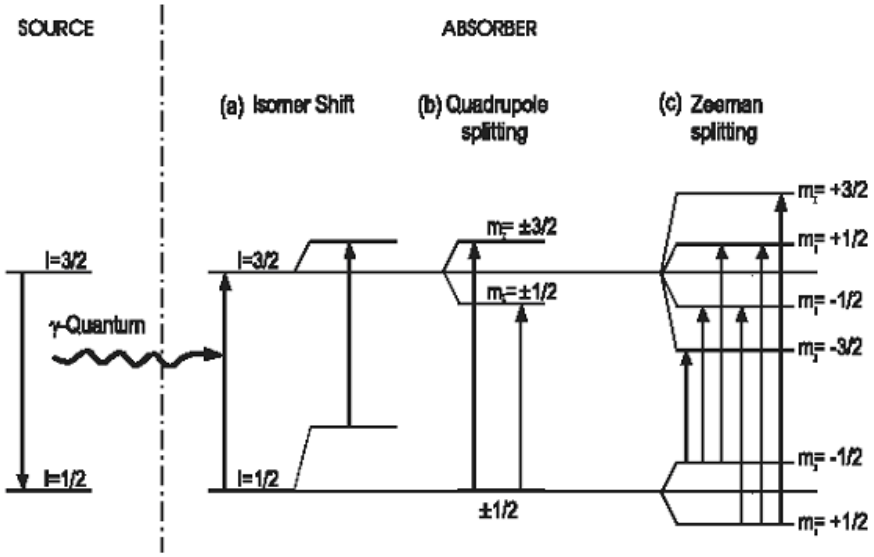


Figure2.3: Hyperfine splitting scheme for the $^{57}$Fe Mossbauer transition induced by (a) Coulomb interaction (isomer shift) (b) Quadrupole interaction and (c) magnetic dipole (Zeeman) interaction between the nucleus and the electrons.

The effective internal field at the nucleus is the result of interaction of the nuclear spin with the spin of the surrounding electrons. The hyperfine magnetic field from a single electron is [**16**]

$$H = -2\mu_B \left[ \frac{8\pi}{3} \psi^2(0)(S) + \left( \frac{1}{r^3} \right) + \left( \frac{3\vec{r}\left(\vec{s}.\vec{r}\right) - r^2\,\vec{s}}{r^5} \right) \right]$$

The first, the second and the third terms are called respectively, the Fermi contact term, orbital angular momentum term, and the dipolar interaction term. The Fermi contact term is non-zero only for S-electrons. However, the other terms representing the dipolar interaction of the electron spin and the orbital term are zero for S-electrons. Since the exchange interaction of a spin up 3d electron with a spin up s-electron is attractive while that with a spin downs-electron is repulsive [**15**], the spin densities due to s-electrons no longer cancel. The net magnetic field [**16**] produced by the Fermi contact term can be written as

$$-2\mu_B \frac{8\pi}{3} \psi^2(0)(S) = -\frac{8\pi}{3} 2\mu_B \Sigma\left(\vec{S}_\uparrow - \vec{S}_\downarrow\right)$$

In a magnetic atom such as Fe, the magnetic 3d electrons polarize the inner s-electrons via the exchange attraction that exists between electrons of like spin. The magnetic 3d electrons are very effective in spin polarizing the 2S electrons. Although their overlap is even greater with the 3S electrons there is partial cancellation since the inner part of the 3S electron density is pulled in a direction opposite to the outer part. The net 4S contribution to the magnetic field is thus positive for the free Iron atom, but the opposite may be true for the 4S conduction band in iron or its alloys, For a free iron atom the fields are about -20,-1300,+700,+500 KOe for 1S,2S,3S, and 4S shells respectively.

The second term in equation (1) is small in many crystals because of quenching of the orbital angular momentum. The third term represents the dipole field due to the electron spin. These two terms are generally smaller than the contact term but in many cases contribute appreciably. Both terms can be positive or negative depending upon the number of electrons and the shape of their charge distribution.

From Zeeman splitting of nuclear levels one determines the hyperfine magnetic field at the nucleus and one can understand connection between hyperfine field at the nucleus and the gross magnetization.

**iv. Line shape and line width**

Resonance absorption shows a characteristic energy dependence of the form [**17**]

$$I(E)=\frac{\Gamma_{ex}}{2\pi}\left[(E-E_t)^2+\left(\frac{1}{2}\Gamma_{ex}\right)^2\right]^{-1}$$

Where $\Gamma_{ex}$ is the experimentally determined full width at half maximum and $E_t$ is the nuclear transition energy. This distribution is known to show a Lorentzian shape. The natural line width of the 14.4 Kev gamma-rays from $Fe^{57}$ is 0.019cm/sec. and is never achieved in practice. This is because of line broadening due to two reasons; one being experimental in origin and other is due to the natural properties of the solid under investigation.

The mechanical vibrations impart undesirable velocities to the source and the absorber which result in the line broadening. A finite solid angle between the source and detector also contributes to the broadening. These can be reduced to some extent by taking special precautions and using stable equipment. Various effects like relaxation effects, inhomogeneous hyperfine interaction, presence of lattice defects which are nonuniformly distributed near the source atom etc., can broaden the Mossbauer lines. Important information about (a) relaxation times (e.g., spin lattice and spin-spin relaxation), (b) diffusion coefficient, (c) lattice defects etc. can be extracted from the observed line broadening if the broadening due to the experimental set up is known.

**d) Fourier transform infrared (FTIR) spectroscopy**

Then energy, E, of electromagnetic radiation is given by the Bohr equation, as

$$E = h\nu \quad \text{---------- 1}$$

where h is the Planck's constant ($h = 6.626 \times 10^{-34}$Js) and ν is equivalent to the classical frequency. Whenever a molecule with quantized discrete energy levels $E_0$, $E_1$, $E_2$, etc interacts with radiation, a quantum of energy (or photon) is either emitted or absorbed. In each case, the energy of the quantum of radiation must be equal to the difference of any two energy levels $E_1$-$E_0$ or $E_2 - E_1$, etc. The energy of the quantum is related to the frequency by the following:

$$\Delta E = h\nu \text{ --------- 2}$$

Hence, the frequency of emission or absorption of radiation for a transition between the energy states and is given by:

$$\nu = \frac{E_1 - E_0}{h} \text{------3}$$

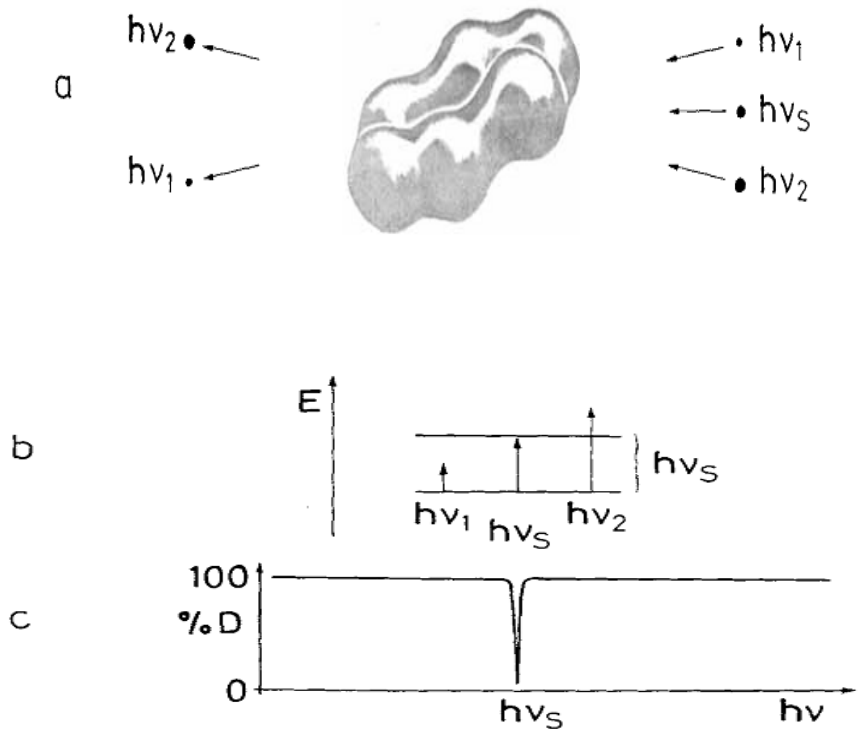


Figure 2.4 Principle of infrared absorption: (**a)** Quanta of the energy $h\nu_1$, $h\nu_S$ and $h\nu_2$ hit the molecule, only $h\nu_S$ is absorbed; (**b**) term diagram; (**c)** infrared absorption spectrum.

Infrared spectra are usually recorded by measuring the transmittance of light quanta with a continuous distribution of the sample. The frequencies of the absorption bands $\nu_S$ are proportional to the energy difference between the vibrational ground and excited states (Fig. 1).

The absorption bands due to the vibrational transitions are found in the wavelength region of $\lambda$ = 2.5 to 1000 µm, which is equivalent to a wavenumber range of $\nu$ = 4000 to 10 $cm^{-1}$.

The interactions of infrared radiation with matter may be understood in terms of changes in molecular dipoles associated with vibrations and rotations. In order to begin with a basic model, a molecule is similar to a system of masses joined by bonds with spring-like properties. Taking first the simple case of diatomic molecules, such molecules have three degrees of translational freedom and two degrees of rotational freedom. The atoms in the molecules can also move relative to one other, that is, bond lengths can vary or one atom can move out of its present plane. This is a description of stretching and bending movements that are collectively referred to as vibrations. For a diatomic molecule, only one vibration that corresponds to the stretching and compression of the bond is possible. This accounts for one degree of vibrational freedom.

Polyatomic molecules containing many (N) atoms will have 3N degrees of freedom. Looking first at the case of molecules containing three atoms, two groups of tri-atomic molecules may be distinguished, i.e. linear and non-linear. Two simple examples of linear and non-linear tri-atomics are represented by $CO_2$ and $H_2O$, respectively. Both $CO_2$ and $H_2O$ have three degrees of translational freedom. Water has three degrees of rotational freedom, but the linear molecule carbon dioxide has only two since no detectable energy is involved in rotation around the O = C = O axis. Subtracting these from 3N, there are 3N-5 degrees of freedom for $CO_2$ (or any linear molecule) and 3N-6for water (or any non-linear molecule). N in both examples is three, and so $CO_2$has four vibrational modes and water has three. The degrees of freedom for polyatomic molecules are summarized in Table 1.

Table 1 Degrees of freedom for polyatomic molecules.

| Type of degrees of freedom | Linear | Non-linear |
|---|---|---|
| Translational | 3 | 3 |
| Rotational | 2 | 3 |
| Vibrational | $3N-5$ | $3N-6$ |
| Total | $3N$ | $3N$ |

Whereas a diatomic molecule has only one mode of vibration which corresponds to a stretching motion, a non-linear B–A–B type tri-atomic molecule has three modes, two of which correspond to stretching motions, with the remainder corresponding to a bending motion. A linear type tri-atomic has four modes, two of which have the same frequency, and are said to be degenerate.

Two other concepts are also used to explain the frequency of vibrational modes. These are the stiffness of the bond and the masses of the atoms at each end of the bond. The stiffness of the bond can be characterized by a proportionality constant termed the force constant, k (derived from Hooke's law). The reduced mass, μ, provides a useful way of simplifying our calculations by combining the individual atomic masses, and may be expressed as follows:

$$\frac{1}{\mu} = \frac{1}{m_1} + \frac{1}{m_2} \quad \text{- - - - - - - 4}$$

where $m_1$ and $m_2$ are the masses of the atoms at the ends of the bond. A practical alternative way of expressing the reduced mass is:

$$\mu = \frac{m_1 m_2}{m_1 + m_1} \quad \text{- - - - - - - 5}$$

The equation relating the force constant, the reduced mass (μ) and the frequency (ν) of absorption is:

$$\nu = \frac{1}{2\pi}\sqrt{\frac{k}{\mu}} \quad \text{- - - - - - - - - 6}$$

This equation may be modified so that direct use of the wave number ( $\bar{\nu}$ ) values for bond vibrational frequencies can be made, namely:

$$\bar{\nu} = \frac{1}{2\pi c}\sqrt{\frac{k}{\mu}} \quad \text{- - - - - - - - - 7}$$

Where c is the speed of light.

A molecule can only absorb radiation when the incoming infrared radiation is of the same frequency as one of the fundamental modes of vibration of the molecule. This means that the vibrational motion of a small part of the molecule is increased while the rest of the molecule is left unaffected.

Infrared absorptions are not infinitely narrow and there are several factors that contribute to the broadening. For gases, the Doppler Effect, in which radiation is shifted in frequency when the radiation source is moving towards or away from the observer, is a factor. There is also the broadening of bands due to the collisions between molecules. Another source of line broadening is the finite lifetime of the states involved in the transition. From quantum mechanics, when the Schrodinger equation is solved for a system which is changing with time, the energy states of the system do not have precisely defined energies and this leads to lifetime broadening. There is a relationship between the lifetime of an excited state and the bandwidth of the absorption band associated with the transition to the excited state, and this is a consequence of the Heisenberg Uncertainty Principle. This relationship demonstrates that the shorter the lifetime of a state, then the less well defined is its energy.

An inspection of infrared spectra shows two absorption bands below $1000cm^{-1}$ as a common feature of all ferrites. The bands arise from lattice vibrations of the oxide ions against the cations. At higher frequencies gradually increasing absorption caused by electronic transitions is observed. The vibrational mode of tetrahedral sites is higher as compared to that of octahedral sites, which is attributed to the shorter bond length of tetrahedral clusters. Any change in the mean ionic charge at sites or the bond length between oxide ions and the cations result a change in the force between the ions leading to a change in the force constant and hence a change in the wave number.

The goal of the basic infrared experiment is to determine changes in the intensity of a beam of infrared radiation as a function of wavelength or frequency (2.5 - 50 µm or 4000 – 200 $cm^{-1}$ respectively) after interaction with the sample. The function of source is to disperse the light from a broadband infrared source and spectrometer measures the intensity at each frequency. The ratio of the intensity before and after the interaction of light with the sample is determined.

**B.Magnetic Properties**

**a) Saturation magnetization**

Saturation magnetization, $M_S$, of a material is the resultant of dipole moments per unit volume when the dipole moments associated with all the molecules are aligned in the direction of the applied magnetic field, and is given by

$M_s = N \mu_m$

where N is number of dipoles and $\mu_m$ is the dipole moment.

A magnetic ferrite crystal has a domain structure similar to that of ferromagnetic metals. The magnetization of each domain is associated with the magnetic moments of the constituent ions. Considering the contribution to the magnetic moment from the individual ions present in the ferrite, the free oxygen atom has a partially unfilled 2P-sub shell which gets filled on acquisition of two electrons when free oxygen converts to $O^{2-}$ negative ion. The oxygen ions therefore have no magnetic moment and so make no direct contribution to the magnetic moment of the domain. The magnetic moments of the remaining ions arise from unfilled outer sub-shells. As in ferromagnetic metals and in paramagnetic solids the moments due to the orbital motions of the electrons are quenched by internal fields, i.e., they are not oriented by externally applied fields, the ionic magnetic moments are therefore due to parallel uncompensated electron spins in the ions. In the case of an iron atom there are four uncompensated spins in the 3d-sub shell, so that the iron atom, assuming quenched orbits, has a magnetic moment of 4 $\mu_B$ ($\mu_B$ being the Bohr-magneton) due to spin. The divalent iron ion having lost two electrons from the 4S shell has a moment of 4 $\mu_B$. On becoming trivalent it loses an addition electron from the 3d sub shell increasing the uncompensated electron spins to 5 and the resultant moment becomes 5 $\mu_B$.

Between the spinning electrons in the neighboring metal ions strong quantum mechanical forces of interaction occur. In ferrites, according to Neel [**18**], there exist three kinds of exchange interactions; the interaction between the various magnetic ions located at A-site (AA interaction), the interaction between the various magnetic ions located at B-site (BB interaction), and the interaction of magnetic ions at A-site with those at B-site (AB interaction); of these AB interaction predominates in strength over AA and BB interactions. These interactions align all

the magnetic spins at A-site in one direction and those at B-site in the opposite direction. The net magnetic moment of the lattice is therefore the difference between the magnetic moments of B and A sublattices,

i.e., $\mathbf{M = M_B - M_A}$.

From the experimentally measured saturation magnetic moment per unit mass $\sigma_s$, the saturation magnetization $M_S$ (magnetic moment per unit volume) and the number of Bohr-magnetons per formula, $n_B$, can be obtained using the following relations [**18**]

$$M_S = \sigma_s d \text{ and } n_B = \frac{\sigma_S M}{5585}$$

where d is density of the sample in gm/cm$^3$ and M is the molecular weight in gm/mol.

The magnetization measurements would provide useful information in understanding the cation distribution of given composition and the role of exchange interactions among the cations lying on A and B sites of spinel lattice.

**b) Initial permeability**

Like all ferromagnetic substances ferrites exhibit hysteresis. The ratio of magnetic induction (B) to applied magnetic field (H) at a point on hysteresis loop represents the state of magnetization of the material, called the permeability of the material, and is written as

$$\mu = \frac{B}{H}$$

Permeability is the degree of magnetization that a material obtains in response to an applied magnetic field. For most of the magnetic core applications, the permeability at very low magnetic fields is of interest which is sometimes referred to as the initial permeability [**19**]. The knowledge of initial permeability is useful in understanding the effective use of the material for core applications over a wide range of frequency and temperatures. A reduction in size and increase in operational frequency of a magnetic core can be made possible by increasing the initial permeability.

**c) Curie temperature**

Magnetic properties of materials arise from uncompensated electron spins that result in a net magnetic moment. As mentioned in Sec.2.3, according to Neel [**20**] in ferrites there exist three kinds of exchange interactions between various ions at A and B sites, namely, AB, BB and AA interactions. The net magnetic moment of the lattice is the difference between the magnetic moments of B and A sub lattices. Perfect alignment of magnetic spins of all molecules is possible only at $0^{o}$K. Randomizing effects of thermal motion cause magnetic moments to decrease as temperature increases from 0 K; this rate of decrease becomes more rapid as the temperature nears the Curie point. The Curie point is the temperature at which the aligning effect of the exchange interaction is cancelled by the disordering effect of random thermal motion.

$$E_J = E_{thermal}$$

That is, $-2I_J Z S^2 = -g S \mu_B H_{eff} = 3 KT$,

Where $H_{eff}$ = effective magnetic field, $E_J$ = exchange energy, Z = number of near neighbours and S = spin quantum number. From the equations it is obvious that the Curie points are proportional to the exchange integral and the number of nearest magnetic neighbours. Curie temperatures increase as the number of spins per atom increases and this increased spin results in a stronger interaction between the neighbouring magnetic ions. The idea of Curie temperature gives an estimate of the temperature at which the device can be operated safely.

References


1. S. Zahi, A.R. Daud and M. Hashim, *Mater. Chem. Phys.* 106 (2007) 452.
2. A. Mahesh Kumar, M. Chaitanya Varma, Charu Lata Dube, K.H. Rao, Subhash C. Kashyap, *J. Magn. Magn. Mater.* 320 (2008) 1995.
3. A Fairweather , F F Roberts and A J E Welch, Rep. Prog. Phys. **15** (1952) 142.
4. EC Snelling, *Soft ferrites: Properties and Applications, second Ed. Butterworths* (1988).
5. M. Tokonami and H. Horiuchi *Acta Cryst.* A36 (1980) 122-126.
6. Q Wei, J Li, Y Chen and Y Han *Mater. Charact.* 47 (2001) 247.
7. AL Stuijts and C Kooy *Sci. Ceram.* **2** (1965) 231.
8. R F Sohoo, Theory and Applications of Ferrite Englewood Cliffs, NJ: Princeton-Hall (1960) p.24.
9. R. L. Mössbauer and D. H. Sharp, *Rev. Mod. Phys*. 36 (1964) 410.
10. BD Cullity and SR Stock "*Elements of X-ray diffraction*" third edition, Prentice Hall Inc. (2001) p.158.
11. RL Mossbauer Z.Phys . 151, (1958) 124.
12. R L Mössbauer *Annual Review of Nuclear Science* 12 (1962) 123-152.
13. P. Gütlich, R. Link and A. Trautwein. *Mössbauer Spectroscopy and Transition Metal Chemistry*, Springer, Heidelberg (1978).
14. P. Gütlich and J. Ensling. In: E.I. Solomon and A.B.P. Lever, Editors, *Inorganic Electronic Structure and Spectroscopy*, Wiley, New York (1999) 161.
15. V.I. Goldanskii,; E.F. Makarov and V.V. Khrapov, *Phys. Letters* 3 (1963) 344.
16. TE Cranshaw, BW Dale, GO Longworth and CE Johnson *Mossbauer spectroscopy and its applications* (1985) Cambridge Universtiy Press.
17. G. Lang, *Nuclear Instruments and Methods* 24 (1963) 425.
18. L Neel *Ann. Geophys.* **5** (1949) 99.
19. EW Gorter *Philips. Res. Rep.* **9** (1954) 321.
20. Syôhei Miyahara, *J. Phys. Soc. Japan.* **5** (1950) 8.